ACS Sustainable Chemistry & Engineering

Research Article

pubs.acs.org/journal/ascecg

Nitrogen Doping of Hydrochars Produced Hydrothermal Treatment of Sucrose in H_2O, H_2SO_4, and NaOH

K. G. Latham,[†] G. Jambu,[‡] S. D. Joseph,[†] and S. W. Donne[†,*]

[†]Discipline of Chemistry, University of Newcastle, Callaghan, NSW 2308, Australia

[‡]School of Engineering, University of Nantes, Rue Christian Pauc, CS 50609, 44306 Nantes, Cedex 3, France

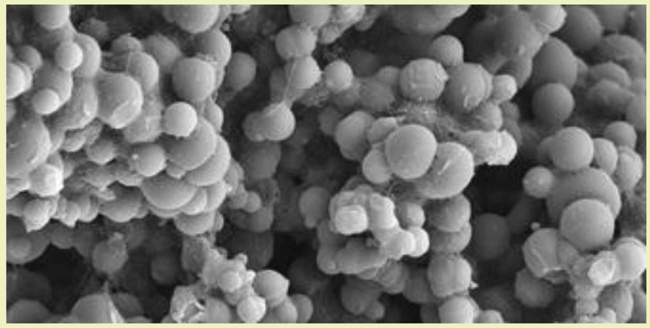

ABSTRACT: In this work, we have focused on the effect of highly acidic (0.2 M H_2SO_4), neutral (H_2O), and basic (0.2 M NaOH) solutions with and without the addition of 0.2 M $(NH_4)_2SO_4$ on the chemical and structural morphologies of hydrothermally formed carbon spheres (hydrochar) from sucrose at 200 °C for 4 h. Hydrolysis product yields without the addition of $(NH_4)_2SO_4$ varied considerably (11.34 wt % H_2SO_4, 47.81 wt % H_2O, and 3.54 wt % NaOH) as did spherical size (3.34, 4.57, and 6.63 nm for H_2SO_4, H_2O, and NaOH, respectively). The addition of $(NH_4)_2SO_4$ increased product yields considerably in acidic and basic conditions (27.76 wt % H_2SO_4 and 14.73 wt % NaOH). Chemically, the hydrochars had a carbon content between 60 and 70 wt % and oxygen content between 22% and 29% with alcohol groups (12.29, 15.44, 11.26 atom % for H_2SO_4, H_2O and NaOH respectively) the main oxygen functionality, although carbonyls, carboxylic acids, and ketones were also present. These oxygen functionalities fluctuated with the presence of $(NH_4)_2SO_4$, with reductions in alcohols (1−3 atom %) and ketones (1−3 atom %), and increases in carboxylic acids. Nitrogen was located in pyridinic, pyrrolyic, and quaternary groups (6.24, 3.22, and 9.41 atom % for H_2SO_4, H_2O, and NaOH, respectively). GC-MS revealed that levulinic acid was the predominate byproduct.

KEYWORDS: *Hydrochar, Sucrose, Hydrothermal carbonization, Amination, Nitrogen doping*

■ INTRODUCTION

The development of carbon materials from renewable sources has been growing in interest in the areas of environmental science and energy storage as a low-cost, environmentally friendly, and nontoxic solution to energy storage, carbon sequestration, environmental remediation, and soil improvement.[1−3] As a result, a number of technologies have been developed to produce novel carbon materials involving approaches such as high temperature pyrolysis, arc discharge, chemical vapor decomposition, and hydrothermal treatment.[4,5] Additionally, the incorporation of nitrogen into carbon materials has been shown to contribute to enhanced electrical conductivity,[6] improved oxidation resistance,[7] changes in adsorption properties, and enhanced agronomic performance.[8−11]

Each of the aforementioned technologies have been developed to incorporate nitrogen into the carbon structure;[6,12−16] however, hydrothermal carbonization holds a particular environmentally advantageous position due to its simple operation and mild reaction conditions,[17] coupled with the ability to exploit renewable biomass with minimal pretreatment as a primary feedstock,[18,19] representing a significant energy saving over the entire process in comparison to other carbonization techniques. Additionally, hydrothermal carbonization yields a number of useful liquid products, such as furfurals, aldehydes, and organic acids,[20,21] which have the potential to be reprocessed into biofuels leaving very few waste products from the carbonization process.[22]

Currently, the hydrothermal carbonization of simple monosaccharide and oligosaccharides has been studied largely under pure water, with minimal investigation performed into the modification of hydrochar through changes in pH or the addition of nitrogen into the hydrothermal reaction. Additionally, studies that have focused on pH modification primarily examined the liquid solution finding that by shifting the pH toward acidic or basic conditions a significant increase in organic acid production occurs. Other recent studies in this field have focused on the effect of various salts on hydrothermal carbonization, finding that both the nature of the cation and anion can have a significant effect on the degree of carbonization, yield, and organic acid production.[23,24]

Therefore, the aim of this study is to understand the effect of acidic and alkaline environments on the hydrochar produced by the hydrothermal carbonization of sucrose using readily available sulfuric acid and sodium hydroxide and then directly comparing them to the hydrochar produced from pure water. As previously stated, the incorporation of nitrogen into the structure enhances a number of desirable properties for

Received: October 23, 2013
Revised: December 9, 2013
Published: December 16, 2013

Table 1. Sample Names, Conditions, Yield, Initial and Final pH of Solutions, Average Carbon Microsphere Size, And Standard Deviation

hydrochar	solution	yield (wt %)	pH initial	pH final	H^+ produced (moles)	average microsphere size (μm)
HW	water + 0.1 M sucrose	47.81	5.4	2.43	0.0037	4.57 ± 1.15
HA	0.2 M H_2SO_4 + 0.1 M sucrose	11.33	0.95	0.81	0.042	3.34 ± 0.59
HB	0.2 M NaOH + 0.1 M sucrose	3.54	13.12	4.27	0.20	0.63 ± 0.21
HWN	water + 0.1 M sucrose + 0.2 M $(NH_4)_2SO_4$	44.41	5.35	1.72	0.019	4.12 ± 0.95
HAN	0.2 M H_2SO_4 + 0.1 M sucrose +0.2 M $(NH_4)_2SO_4$	27.76	1.23	1.09	0.022	4.39 ± 1.20
HBN	0.2 M NaOH + 0.1 M sucrose +0.2 M $(NH_4)_2SO_4$	14.73	9.51	2.17	0.0068	6.03 ± 1.94

carbons, and as such, the potential to nitrogenate the hydrothermal product using ammonium sulfate will also be examined under these conditions.

EXPERIMENTAL SECTION

Raw Materials and Solution Preparation. A 0.2 M H_2SO_4 was prepared from concentrated H_2SO_4 (Sigma Aldrich, 95−98%). Similarly, 0.2 M NaOH was prepared from solid NaOH (Sigma Aldrich, 97% pellets). Nitrogenated solutions were prepared by dissolving solid ammonium sulfate into electrolytes of 0.2 M H_2SO_4, 0.2 M NaOH, or water to give a concentration of 0.2 M $(NH_4)_2SO_4$. Sucrose was also added to each solution until a concentration of 0.1 M sucrose was achieved. All solutions were prepared with Milli-Q ultra pure water (Table 1).

Hydrothermal Treatment. A 350 mL aliquot of the starting solution was placed in a Teflon-lined steel bomb reactor with an internal volume of 450 cm^3. The bomb reactor was then sealed and heated in a furnace at 200 °C for 4 h. This temperature was selected because of the following: (i) A previous study had shown that maximum nitrogen fixation was achieved at 200 °C in comparison to lower temperatures.[25] (ii) The temperature employed is higher than the normal glycosidation temperature of sucrose.[26] (iii) A pilot study (results not included) on reaction time revealed that yield did not substantially increase after 4 h under H_2O at 200 °C. After this time period, the bomb reactor was removed and left to cool to room temperature for 24 h. The solid products were collected by filtration and washed with Milli Q ultra pure water until neutral, and then dried at room temperature to prevent modification of the surface from exposure to atmospheric oxygen at elevated temperatures. The final solid product was weighed after drying to obtain the yield. The liquid phase pre- and post-hydrothermal treatment had its pH tested to determine the overall acid contribution from the hydrothermal process.

Structural Determination and Morphology. *FTIR Analysis.* Infrared spectra were recorded on a Perkin-Elmer spectrum BX FTIR spectrophotometer, collected using 128 scans in the wavenumber range 400−4000 cm^{-1} with a resolution of 2 cm^{-1}. Samples were prepared in KBr (>99.99%, Sigma Aldrich) at a mass ratio of 100:1 KBr:hydrochar and pressed into pellets under a pressure of 738 MPa. Background spectra were recorded between each sample using a blank KBr disk through air and were used to correct each sample spectrum.

X-ray Photoelectron Spectroscopy (XPS) Analysis. XPS was performed using a Thermo ESCALAB250i X-ray photoelecton spectrometer with elemental mapping capability and He UV source.

Elemental Analysis. Elemental analysis was conducted using a PerkinElmer model PE2400 CHNS/O elemental analyzer with a PC-based data system, PE Datamanager 2400, and a PerkinElmer AD-6 ultra micro balance. The instrument was run in CHNS and ash mode in duplicate with a sample size between 1 and 2 mg. Determination of oxygen was performed by the difference between the total CHNS found in the sample and the initial weight.

Morphological Analysis. Hydrochars were mounted on aluminum stubs with double-sided carbon tape and gold coated before being examined with a Philips XL30 scanning electron microscope (SEM) at different magnifications. To determine the size distribution of the synthesized microspheres, the diameters of around 100 particles (as visualized by SEM) were measured at a set working distance.

TGA Analysis. Thermogravimetric analysis (TGA) was performed on 4−6 mg of hydrochar in a ceramic alumina pan with a second reference pan containing 4−6 mg of powdered alumina (α-Al_2O_3). The temperature program was set to a rate of 5 °C/min to reach a final temperature of 1000 °C on a PerkinElmer Diamond TG/DTA. Experiments were performed under a continuous flow of nitrogen at a rate of 50 mL/min.

Chromatographic Analysis of Supernatant Liquid. After separation of the hydrochar from the supernatant liquid, a 1 μL sample of the filtrate was injected into a Shimadzu GC-MS QF2010 EI/NCI system fitted with a ZB-5MS column (30 m × 0.25 mm) with a 5% phenyl-arylene stationary phase. A temperature program was set to rest at 45 °C for 5 min before increasing in temperature at 10 °C/min until 200 °C was reached, where it was again rested for 5 min. Qualitative compound determination was performed by comparing the resulting mass spectra to the NIST 07 database. Quantitative analysis was performed on 5-hydroxymethylfurfural and levulinic acid using calibration standards prepared from pure samples obtained from Sigma Aldrich.

RESULTS AND DISCUSSION

Yield and Liquid Solution. The yields of hydrochar for the nitrogenated (HWN, HAN, HBN) and non-nitrogenated (HW, HA, and HB) hydrothermal solutions are presented in Table 1, along with the pre- and post-hydrothermal solution pH. The yield of hydrochar can be seen to vary significantly between each of the non-nitrogenated solutions, with both the acidic and basic solutions producing significantly less hydrochar than the neutral solution. Additionally, significant changes in pH were observed between the pre- and post-hydrothermal solutions, with each solution dropping in pH as a result of hydrothermal carbonization, indicating the production of organic acids. This result was expected, as the hydrothermal carbonization of saccharides produces a number of organic acids, such as acetic, levulinic, formic, and lactic, in addition to organic decomposition products such as furfurals, aldehydes, and phenols.[20,27]

To determine the nature of any organic compounds remaining in the supernatant liquid, the solutions were qualitatively analyzed by GC-MS to determine the identity of any remaining compounds or acids and quantitatively analyzed for 5-hydroxymethylfurfural (HMF) and levulinic acid due to the direct relationship between HMF forming either hydrochar or levulinic acid (Table 2).[5,20,21] As a result, levulinic acid was found in the neutral (3.4 mM), acidic (10.2 mM), and basic (24.74 mM) solutions in increasing concentrations. Additionally, formic acid was also detected in the acidic solution, while the basic solution contained formic, acetic, and lactic acids, as well as levulinic acid.

The increase in concentration of levulinic acid, on top of the increase in the number of acidic compounds detected, explains the significant reduction in hydrochar yield in the acidic (HA) and basic (HB) solutions, as these solutions have clearly shifted the reaction toward the production of acidic products, which

Table 2. Qualitative and Quantitative GC-MS Results for Hydrothermal Solutions Post Reaction

hydrochar	HMF (mM)	levulinic cid (mM)	other compounds detected
HW	0	3.4	furfural, 5-methylfurfural
HA	0	10.20	formic acid, 5-methylfurfural
HB	0	24.74	acetic acid, formic acid, lactic acid
HWN	33.67	0.99	acetic acid
HAN	27.88	9.58	formic acid, oxalic acid
HBN	17.58	16.66	acetic acid, formic acid, methylpyrazine

subsequently prevents the formation of hydrochar.[28,29] Finally, no HMF is detected in any of these solutions, suggesting that the reaction has gone to completion, as hydrochar and levulinic acid are the final outcomes of the hydrothermal carbonization of HMF.

The addition of ammonium sulfate increased the yield in both the acidic and basic solutions, whereas very little change was observed in the neutral solution. Again, similar changes in pH were observed between the pre- and post-reaction solutions, indicating the presence of organic acids, although the initial pH of the basic solution dropped significantly due to neutralization with NH_4^+.

Furthermore, GC-MS analysis of the nitrogenated solutions revealed that levulinic acid was again present in the final solution, although the concentration was slightly lower than the non-nitrogenated solutions. Additionally, HMF was also

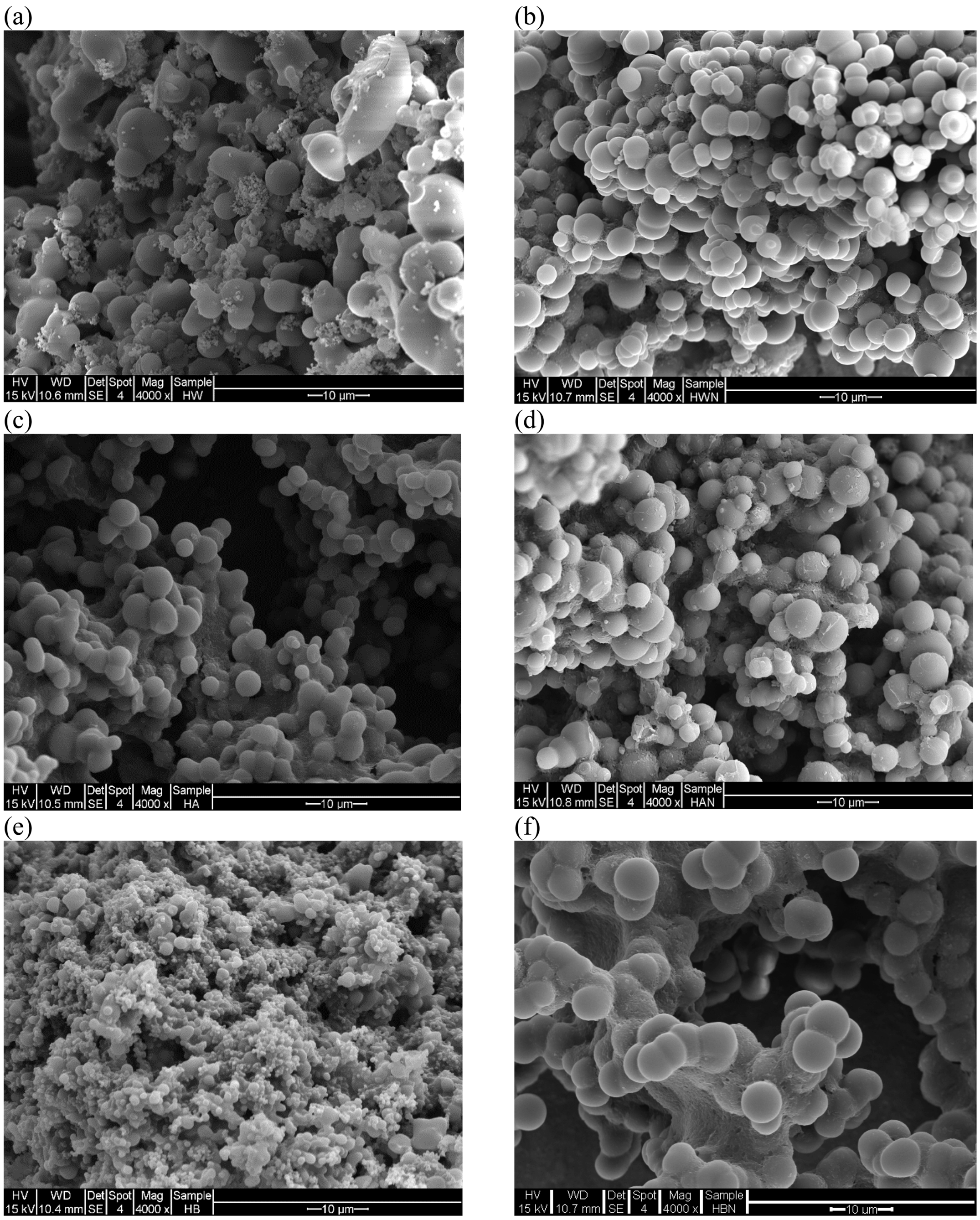

Figure 1. SEM images of (a) HW, (b) HWN, (c) HA, (d) HAN, (e) HB, and (f) HBN at 4000×.

Table 3. Peak-Fitting Results of XPS C1s, N1s, O1s, S1s, Si1s, and F1s Spectra with Detected Functional Groups under C1s and N1s

	band (eV)													
	C (atom %)						N (atom %)			O (atom %)	S (atom %)	Si (atom %)	F (atom %)
	284.9	286.2–288.0	287.2–288.1	288.0–289.2	289.0–291.6		389.5	400.5	401.5	532	168.5	98.3	688.3
hydrochar	nonfunctional	C–OH	–C=O	–COOH	$-CO_3$	total	pyridinic	pyrrolyic	quaternary				
HW	52.88	15.44	5.03	0.33	2.71	76.39	–	–	–	22.8	–	0.26	0.57
HA	56.58	12.29	3.76	2.64	2.83	78.1	–	–	–	20.61	0.1	0.37	0.82
HB	60.54	11.26	4.09	1.31	2.54	79.74	–	–	–	18.78	–	0.32	1.17
HWN	56.65	12.39	2.29	1.05	2.23	74.61	2.13	1.23	2.88	16.62	0.97	0.44	1.14
HAN	54.68	12.15	3.13	1.4	2.68	74.04	0.71	0.79	1.72	19.55	0.76	0.38	1.05
HBN	61.43	9.34	2.55	1.81	2.07	77.2	6.03	1.44	1.94	12.86	0.36	0.42	0.74

Table 4. Elemental Analysis of Hydrochars and O:C and N:C Ratios Calculated from Elemental Analysis and XPS Data

	wt %							elemental analysis		XPS	
sample	C	H	N	S	O	ash	empirical formula	O:C	N:C	O:C	N:C
sucrose[a]	42.11	6.48	0	0	51.41	0	$CH_{1.83}O_{0.92}$	–	–	–	–
HW	65.725	4.80	<0.05	0.58	28.895	<0.01	$CH_{0.87}O_{0.33}$	0.33	–	0.30	–
HA	66.105	4.805	<0.05	0.715	28.375	<0.01	$CH_{0.87}O_{0.32}$	0.32	–	0.26	–
HB	70.34	6.17	<0.05	0.865	22.625	<0.01	$CH_{1.05}O_{0.24}$	0.24	–	0.23	–
HWN	62.495	6.08	6.7	1.07	24.655	<0.01	$CH_{0.97}N_{0.091}O_{0.29}$	0.30	0.09	0.22	0.08
HAN	63.47	4.69	3.26	1.195	27.385	<0.01	$CH_{0.88}N_{0.044}O_{0.32}$	0.32	0.04	0.26	0.04
HBN	60.135	5.43	10.13	0.98	23.325	<0.01	$CH_{1.08}N_{0.14}O_{0.29}$	0.29	0.14	0.17	0.12

[a]Sucrose values calculated from known empirical ratios and not experimental results.

present in the amininated solution, suggesting that the addition of ammonium sulfate reduces the potential for organic acids to be formed, and as a result, an increase in hydrochar yield was observed. The reasoning behind the increase in yield will be discussed later in correlation with the elemental analysis and XPS results.

Morphology. The hydrochar materials produced under each treatment formed spherical particles with diameters predominately in the 0.5–8 μm range, as evident in the SEM images in Figure 1 of the non-nitrogenated (HW Figure 1a, HA Figure 1b, and HB Figure 1c) and nitrogenated (HWN Figure 1d, HAN Figure 1e, and HBN Figure 1f) hydrochars. Additionally, Table 1 contains the mean and standard deviation on the diameter and distribution of the carbon microspheres. These clearly indicate that in addition to yield of hydrochar, the microspheres in each sample are significantly influenced by the pH of the hydrothermal solution, which is particularly evident when comparing the size of HB with any of the other hydrochars. This size variability is directly related to the acidic and basic hydrothermal solutions promoting the formation of organic acids over hydrochar. As hydrochars form through the processes of nucleation and growth, the increase in organic acids formed under acidic or basic solutions would reduce the levels of hydrochar forming precursors from HMF, thus accounting for the decrease in microsphere size.

Conversely, the nitrogenated hydrochars do not follow the same size pattern as the non-nitrogenated hydrochars, with HBN producing the largest microsphere size and the widest distribution of sizes (3–9.5 μm). The overall increase in size in HAN and HBN again suggests that the addition of ammonium sulfate reduces the catalytic effect of acid or base toward the production of organic acids, allowing increased growth to take place. Additionally, nitrogen is incorporated into the structure (Tables 3 and 4), which may have an additional effect of increasing sphere growth over their non-nitrogenated counterparts. Overall, the variation in microsphere size indicates that it is not only possible to modify the size of the microspheres with temperature and reaction time, as indicated by Sevilla and Furtes,[21] but also by modifying the initial pH of the solution and the addition of NH_4^+.

Chemical Structure and Analysis. The FTIR spectrum for sucrose, $(NH_4)_2SO_4$, and non-nitrogenated and nitrogenated hydrochars are shown in Figure 2. The bands identified in the FTIR spectra of sucrose were assigned to (i) 3395 cm^{-1} to O–H stretch, (ii) 2950 cm^{-1} to C–H stretch, (iii) 1460–1200 cm^{-1} to C–H and O–H deformations, (iv) 1160–1000 cm^{-1} to C–O stretch, and (v) 960–730 cm^{-1} to C–H deformations. The bands identified within the FTIR spectra of ammonium sulfate were assigned to (i) 3300–3030 cm^{-1} to $N-H^+$ stretch and 1419 cm^{-1} to $N-H^+$ deformation in NH_4^+ and (ii) 1120 and 621 cm^{-1} to SO_4 stretch and 1202 cm^{-1} to HSO_4^-asymmetric SO_3 stretch. The primary differences in the FTIR spectra for sucrose and the hydrochars is the appearance of peaks at 1705 cm^{-1} relating to the C=O stretch from ketones, aldehydes, quinones, esters, and carboxylic acids, and at 1625 cm^{-1} from aromatic carbon C=C ring stretches. Additionally, peaks at 2900 and 1000–1200 cm^{-1} are significantly reduced in the hydrochar samples indicating a loss of C–H and C–O–C, which is confirmed in the percentage of C, O, and H contained in sucrose and the hydrochars (Table 3). Although previous studies have indicated that hydrochars do contain C–O functional groups,[30] hydrochar is unlikely to contain the same degree of C–O bonding as sucrose (three C–O–C bonds per molecule).

Examining the differences between the non-nitrogenated and nitrogenated hydrochars, a major reduction in the peak at 1705 cm^{-1} can be seen indicating that nitrogenation of the hydrochar has reduced the formation of C=O groups. A minor band at

dx.doi.org/10.1021/sc4004339 | ACS Sustainable Chem. Eng. 2014, 2, 755–764

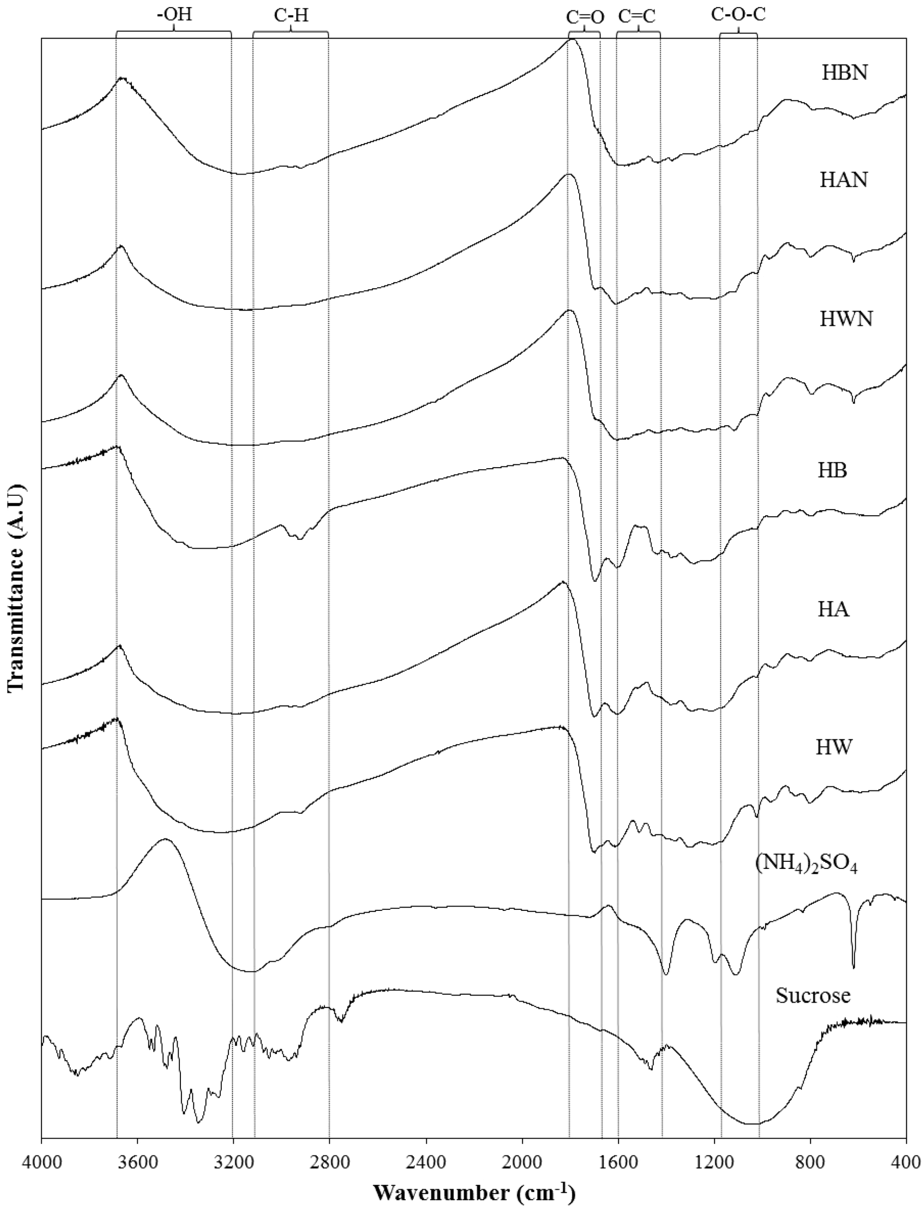

Figure 2. FTIR spectrum of sucrose, $(NH_4)_2SO_4$, and nitrogenated and non-nitrogenated hydrochars.

621 cm^{-1} attributed to the SO_4 stretch is also observed in each of the nitrogenated hydrochars but was not present in HA, indicating that sulfate contained in the structure is most likely from the addition of ammonium sulfate and not from sulfuric acid. The region between 3000 and 3500 cm^{-1}, where various N−H stretching bands are found, was not easily observed in each of the nitrogenated hydrochars due to the merging of these bands with the broad O−H stretch, which was highly pronounced for hydrochars. Additionally, it was noted that none of the major peaks displayed by ammonium sulfate were observed in the nitrogenated chars indicating that any nitrogen groups present are not in the form of NH_4^+ salts precipitated out on the surface but are in fact structurally bound nitrogen functionalities.

The results of the C1s, N1s, O1s, S1s, Si1s, and F1s peaks from XPS are presented in Table 2 with the high resolutions scans of C1s and N1s presented in Figures 3 and 4. The percentage of nonfunctional carbon (52.88% for HW and 60.54% for HB) and carbon/oxygen functionalities are seen to change slightly from acid to base, with HW having the lowest nonfunctionalized carbon content but rich in alcohols (15.44%) and ketones (5.03%). HA has the highest number of carboxyls (2.64%) and carbonates (2.83%), whereas HB contained the lowest level of alcohols (11.26%) but the highest non-functionalized carbon content.

With the addition of ammonium sulfate, the nitrogenated hydrochars shown in Table 2 display an overall loss in C−O functionality on the surface, with HWN displaying the largest loss of oxygen (5.55%) followed by HBN (4.43%) and last HAN (1.16%). In HWN and HBN, alcohol and ketone groups experienced the highest degree of loss, with carbonates remaining relatively unchanged and carboxyl groups increasing a small amount. Conversely, HAN lost entire carbonyl groups, with the other oxygenated functionalities remaining relatively unchanged.

The elemental analysis for C, H, N, S, O, and ash, calculated empirical composition, and the O:C and N:C ratios from elemental analysis and XPS for each of the hydrochars are

dx.doi.org/10.1021/sc4004339 | ACS Sustainable Chem. Eng. 2014, 2, 755−764

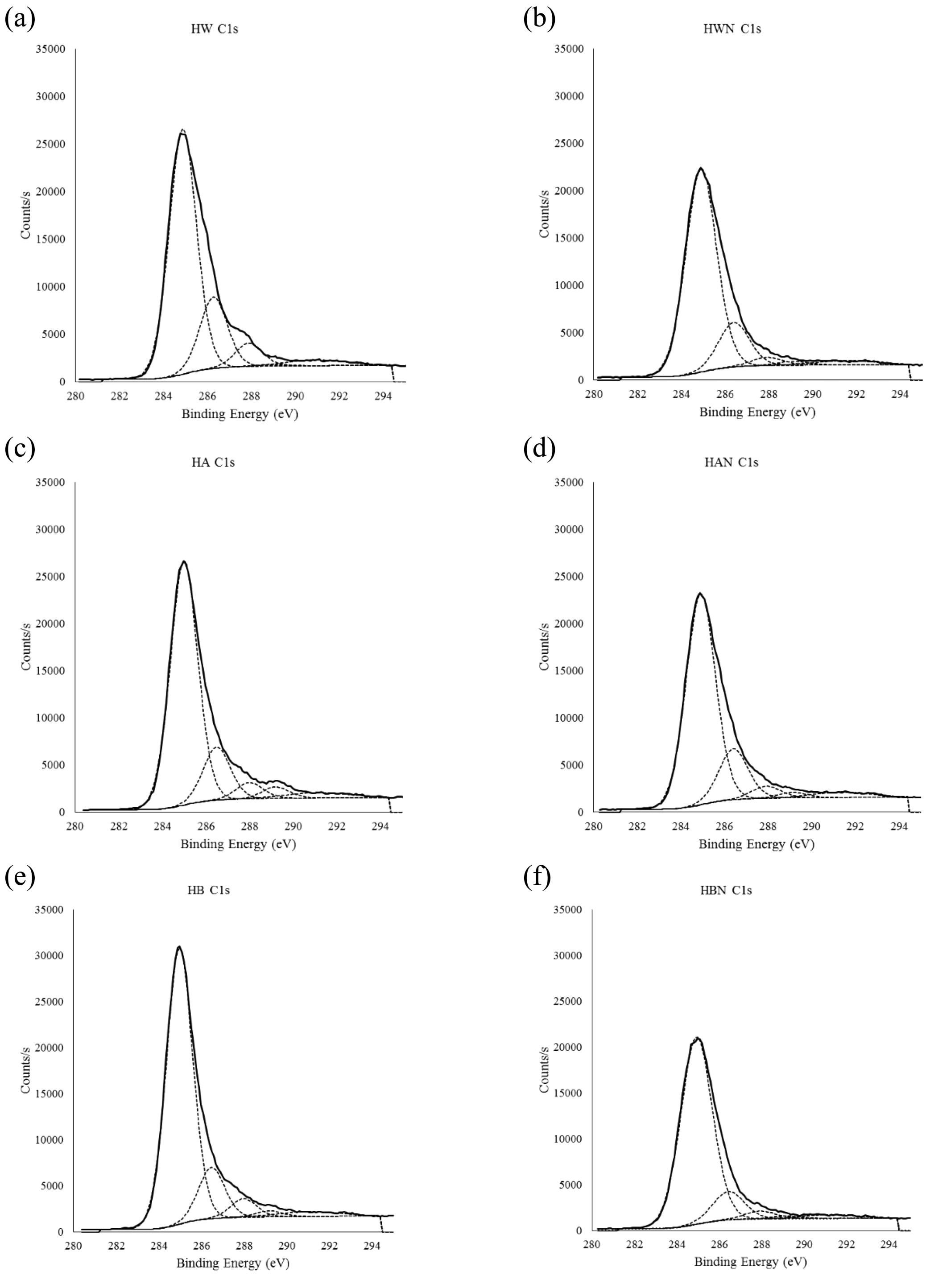

Figure 3. XPS high resolution C1s scans of (a) HW, (b) HWN, (c) HA, (d) HAN, (e) HB, and (f) HBN.

displayed in Table 3. The elemental analysis correlates with previous results that showed that the carbon content increased to around 50–70%, while the oxygen and hydrogen content decreased to around 20–30% and 3–5%, respectively.[21,31−33] Again, there are subtle differences between each of the hydrochars, displaying similar elemental ratios to that of the XPS results.

To examine the difference between oxygen and nitrogen located in the core or on the surface, a direct comparison of the O:C and N:C atomic ratios determined by elemental analysis (core) and XPS (surface) was used (Table 3). In general, the O:C ratio located at the surface of the non-nitrogenated hydrochars was less than that of the core, which contradicts the ratios found in hydrochars made from glucose, cellulose, fructose, and other saccharides, as these have been found to have higher degrees of oxygen located at the surface than in the core. This reversal in oxygen content was also reported by Sevilla and Fuertes for sucrose, although no reason for its existence was given.[21]

In examining the O:C and N:C ratio of the nitrogenated chars, the same drop in oxygen located within the core and the surface was observed, although interestingly there is very little difference between the N:C ratios, suggesting that nitrogen is fully incorporated throughout the hydrochar structure.

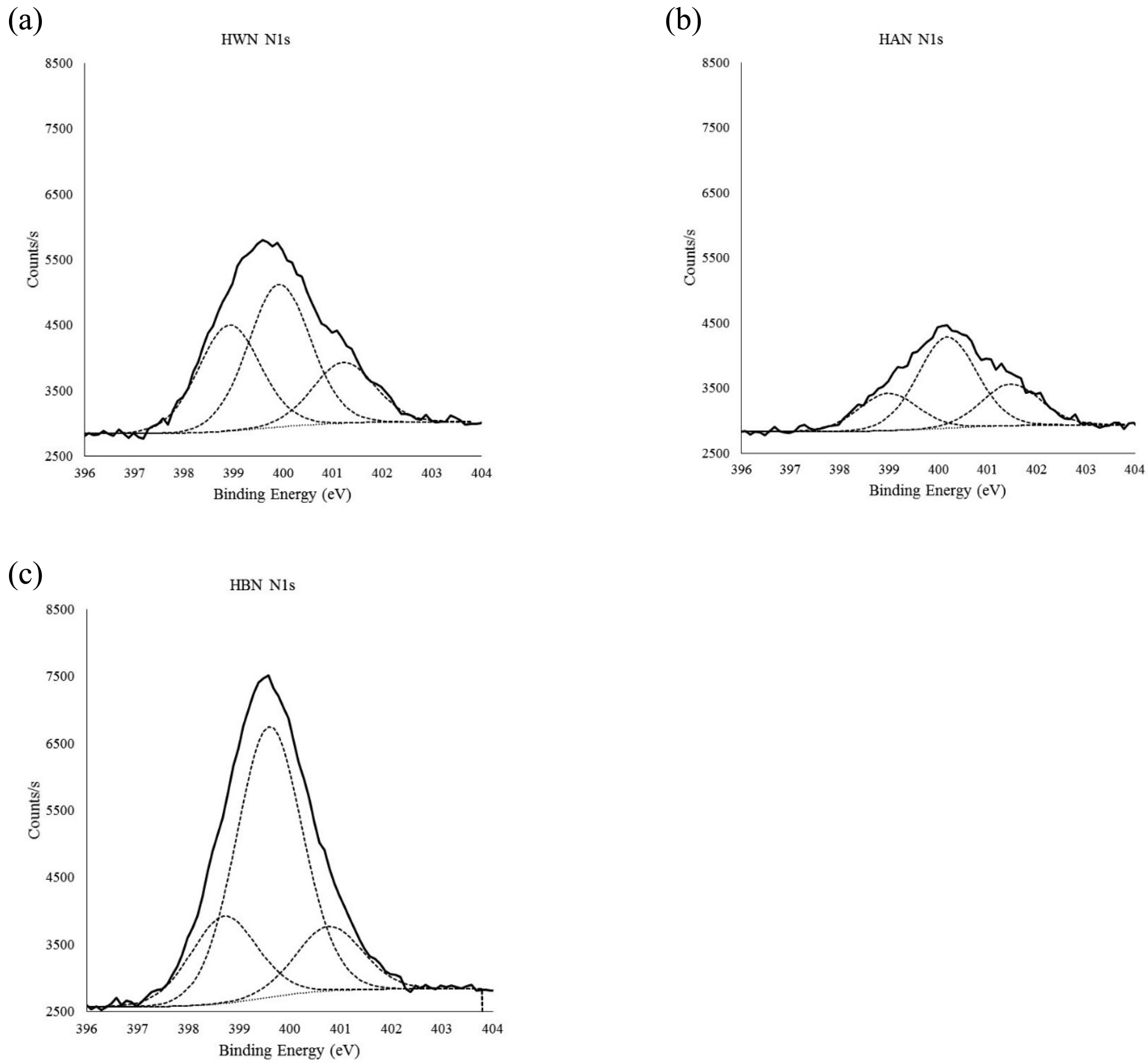

Figure 4. XPS high resolution N1s scans of (a) HWN, (b) HAN, and (c) HBN.

To compare the nature of the initial and final materials, thermogravimetric analysis (TGA) of sucrose and ammonium sulfate are shown in Figure 5. It is shown that sucrose undergoes three mass loss steps, with the first mass loss (30–100 °C) due to the removal of surface bound water, the second mass loss (220–280 °C) due to the decomposition of sucrose above its melting point of 186 °C,[34] and the third mass loss (300–900 °C) related to the removal of CO and CO_2 from the remaining structure as it becomes increasingly more aromatized as the temperature increases. In comparison, ammonium sulfate only displays one mass loss between 300–425 °C, which contains three decomposition steps,[35] i.e.,

$$(NH_4)_2SO_4 \rightarrow NH_4HSO_4 + H_2O$$

$$2NH_4HSO_4 \rightarrow (NH_4)_2S_2O_7 + H_2O$$

$$3(NH_4)_2S_2O_7 \rightarrow 2NH_3 + 2N_2 + 6SO_2 + 9H_2O$$

Comparing these to the TGA curves for the non-nitrogenated and nitrogenated hydrochars (Figure 6), it is shown that the decomposition curves are completely different indicating that the hydrothermal treatment has completely incorporated and rearranged the structure of both materials.

To analyze the hydrothermal TGA curves, the mass loss for the hydrochars needs to be split into three main regions, namely, 80–110, 250–500, and >500 °C. The first mass loss region (80–110 °C) is due to the desorption of physisorbed surface water, the second (250–500 °C) is due to the rearrangement and decomposition of the furan structure, as well as loss of surface functionality, and the final mass loss step (>500 °C) is a result of increasing aromatization of the hydrochar through the removal of oxygen.

Each of the TGA curves of the non-nitrogenated hydrochars display similar decomposition shapes with the main mass loss occurring between 300–500 °C. Despite these similarities, the actual mass loss is vastly different, with HA and HB losing 10–30% more mass than HW. As both of these hydrochars contain lower degrees of carbon/oxygen surface functionalities than HW, the increase in mass loss must be a result of the decomposition of the carbon structure, suggesting that the main structural motif is indeed weaker than in HW.

Interestingly, the nitrogenated hydrochars display almost identical TGA profiles with mass losses similar to that of HW, suggesting a similar structural motif across all three nitrogenated hydrochars and that the incorporation of ammonium sulfate reduces the negative impact on structure formation under acidic and basic conditions.

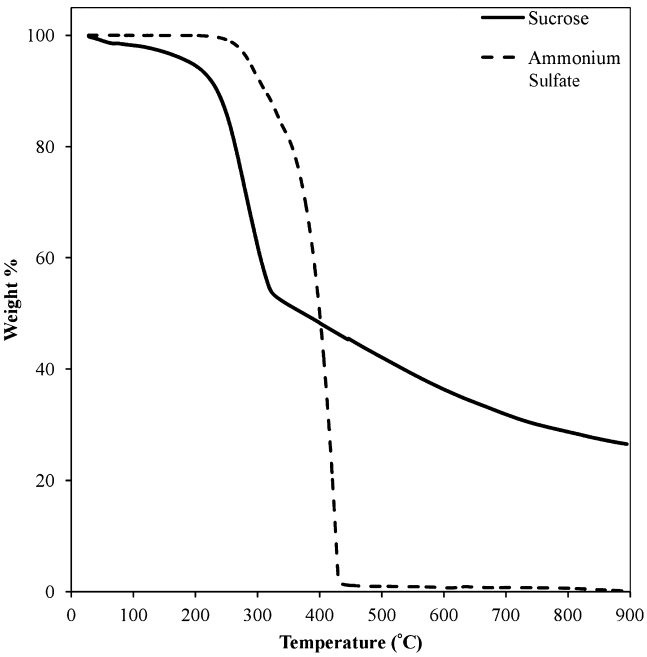

Figure 5. TGA of sucrose and ammonium sulfate under N_2 at 5 °C/min.

Effect of pH on Non-Nitrogenated Hydrochars. It has been previously stated that the autohydrolysis of water into H^+ and OH^- is responsible for the hydrolysis reactions that take place under hydrothermal carbonization.[21,36] Under neutral conditions, the concentration of H^+ and OH^- produced from water at 200 °C is 2.213×10^{-6} mol/L,[37] but under highly acidic conditions, only H^+ would factor into the hydrolysis reactions, as OH^- produced from water would be quickly neutralized. The opposite would occur in the basic solution, with H^+ being quickly neutralized by the excess of OH^-. As a result, the differences in surface and core oxygen content, yield, functionality, and size for the non-nitrogenated hydrochars are a direct result of the increase in H^+ or OH^- within the solution, which in turn influenced the competing reaction pathway and reaction rates of glucose and fructose and their subsequent decomposition products..

To examine this, the formation of HMF, which has been shown to form the main furan core, can be used to gauge how acidic, basic, and neutral solutions effect hydrochar formation. In terms of reaction rate, fructose not only produces HMF faster than glucose but also at higher concentrations under acidic, neutral, and basic environments.[38] This is due to glucose forming HMF primarily through epimerization to fructose, with its subsequent decomposition to HMF.[20] As a result, glucose produces higher quantities of products such as glycoaldehyde and 1,6-anhydroglucose. Therefore, it would be reasonable to assume that the initial hydrothermal structure consists of decomposition products predominately from fructose, whereas later stages of the carbonization would incorporate those which come from glucose decomposition and oxygen depleted fructose decomposition products,[20] thus accounting for the difference in oxygenation between the core and the surface under neutral and acidic conditions (HW and HA).

In regards to hydrothermal formation, the aromatized hydrothermal carbon structure is predominately constructed through inter- and intra-molecular dehydration, aldol condensation, keto−enol tautomerism, and ester reactions,[5,21,39] all of which are acid catalyzed reactions. Thus, it would be expected that under acidic conditions, the formation of hydrochar should be greater than under neutral conditions. As this is not apparent, and a reduction in yield, particle size, and oxygen content is actually observed, along with the concentration of levulinic acid increasing considerably, this suggests that under acidic environments, the decomposition reactions that occur under hydrothermal conditions are shifted toward the production of organic acids at earlier stages before hydrothermal carbonization can take place, thus limiting the formation of hydrothermal carbons. Although it has been suggested that the production of organic acids catalyze the formation of hydrochar,[40] this is clearly not evident under both acidic and basic environments, where an increase in organic acid production actually decreases the formation of hydrochar considerably.

This decrease in in yield, size, and oxygen content at both extremes of the pH scale indicates that the process of hydrothermal carbonization, in regards to sucrose, is sensitive to pH, allowing the possibility of carefully controlling the aforementioned properties and organic acid production through careful alteration of the initial solution pH.

Effect of pH and Ammonium Sulfate on Nitrogenated Hydrochars. The addition of ammonium sulfate to the hydrothermal solutions has a number of effects on the final hydrothermal product. First, the negative impact of acidic and basic solutions toward hydrothermal production is decreased, with an increase in yield and sphere size observed. Second, the concentration of levulinic acid produced also decreases, and HMF is found in the final solution, indicating that potentially the rate of formation of either hydrochar or unwanted side products is reduced. Finally, overall oxygen content is found to decrease at a level very similar to the increase in amination indicating that oxygen functionality is replaced by nitrogen groups.

The reasoning behind the increase in yield and size is potentially due to an increase in reactions that lead to polymerization due to the addition of NH_3 as a nucleophile and the reactivity of nitrogenated compounds. For example, trans-amination converts primary amines to secondary amines via

$$R - NH_2 + R' - NH^- \rightarrow R - NH - R' + NH_2^-$$

liberating a reactive NH_2^- molecule while joining two R groups together.[41] Additionally, the pyrolinic and pyridinic nitrogen groups found in the XPS results could be formed through mechanisms such as the amination of a 1,4-diketone with NH_3, although additional reactions also exist for their formation that may also be possible under hydrothermal conditions.[42] The quaternary ammonium salts also found under XPS are normally formed through the alkylation of tertiary amines using a halide as a leaving group, although under hydrothermal synthesis, a protonated alcohol may serve instead, allowing its formation. Overall, further insight is required to ascertain the exact reactions that are occurring under the influence of nitrogen, although the difference in nitrogenation could be as simple as the acid−base effects on the equilibrium between ammonium sulfate and water, i.e.,

$$(NH_4)_2SO_4 + H_2O \leftrightarrow 2NH_3 + 2H_3O^+ + SO_4^{2-}$$

Thus under acidic conditions, the addition of H^+ would shift the equilibrium left, reducing the available ammonia. The reverse would occur in base, increasing the concentration of

dx.doi.org/10.1021/sc4004339 | ACS Sustainable Chem. Eng. 2014, 2, 755−764

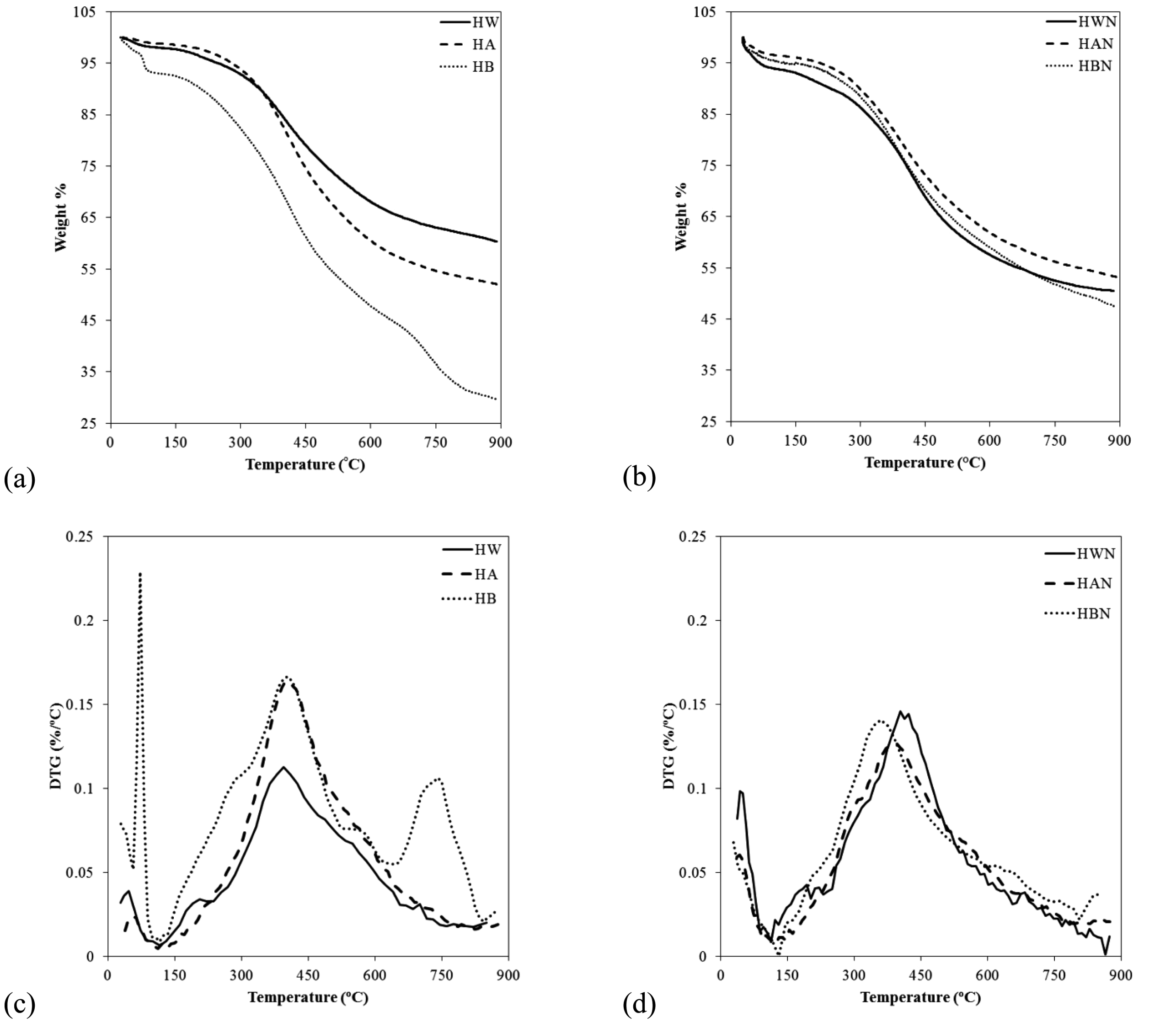

Figure 6. (a) TGA and (b) DTA of non-nitrogenated hydrochars and (c) TGA and (d) DTA of nitrogenated hydrochars under N_2 at 5 °C/min.

ammonia, which in turn would explain why the concentration of nitrogen found in the nitrogenated hydrochars increases with increasing pH.

CONCLUSIONS

In summary, pH was found to drastically effect the yield and morphology of non-nitrogenated hydrochars and under acidic or basic conditions, although minor differences were observed between the elemental composition and surface functionality of each hydrochar in regards to oxygen functionality (22−28%). Upon addition of ammonium sulfate, yield and size increased, with nitrogen content increasing 3-fold by changing the pH from acidic to basic. This increase in nitrogen correlated with a reduction of oxygen content in the nitrogenated hydrochars, suggesting that nitrogen attaches preferentially to oxygen in hydrochar formation, in addition to providing polymerization reactions to the hydrothermal reaction.

AUTHOR INFORMATION

Corresponding Author

*Tel.: +61 2 49215477. Fax: +61 2 49215472. E-mail: scott.donne@newcastle.edu.au.

Notes

The authors declare no competing financial interest.

ACKNOWLEDGMENTS

The authors thank Stephen Joseph (UNSW) for his assistance in obtaining the raw XPS data and the elemental microanalysis service at Macquarie University for the elemental analysis. Also, K.L. acknowledges the University of Newcastle for the Ph.D. Scholarship.

REFERENCES

(1) Sevilla, M.; Macia-Agullo, J. A.; Fuertes, A. B. Hydrothermal carbonization of biomass as a route for the sequestration of CO_2: Chemical and structural properties of the carbonized products. *Biomass Bioenergy* **2011**, *35* (7), 3152−3159.

(2) Joseph, S. D.; Camps-Arbestain, M.; Lin, Y.; Munroe, P.; Chia, C. H.; Hook, J.; van, Z. L.; Kimber, S.; Cowie, A.; Singh, B. P.; Lehmann, J.; Foidl, N.; Smernik, R. J.; Amonette, J. E. An investigation into the reactions of biochar in soil. *Aust. J. Soil Res.* **2010**, *48* (6&7), 501−515.

(3) Liu, X.-M.; Huang, Z. d.; Oh, S. w.; Zhang, B.; Ma, P.-C.; Yuen, M. M. F.; Kim, J.-K. Carbon nanotube (CNT)-based composites as electrode material for rechargeable Li-ion batteries: A review. *Compos. Sci. Technol.* **2012**, *72* (2), 121−144.

(4) Gherghel, L.; Kubeel, C.; Lieser, G.; Radeer, H.-J.; Mulelen, K. Pyrolysis in the mesophase: A chemist's approach toward preparing carbon nano- and microparticles. *J. Am. Chem. Soc.* **2002**, *124* (44), 13130−13138.
(5) Sevilla, M.; Fuertes, A. B. The production of carbon materials by hydrothermal carbonization of cellulose. *Carbon* **2009**, *47* (9), 2281−2289.
(6) Terrones, M.; Ajayan, P. M.; Banhart, F.; Blase, X.; Carroll, D. L.; Charlier, J. C.; Czerw, R.; Foley, B.; Grobert, N.; Kamalakaran, R.; Kohler-Redlich, P.; Ruhle, M.; Seeger, T.; Terrones, H. N-doping and coalescence of carbon nanotubes: synthesis and electronic properties. *Appl. Phys. A: Mater. Sci. Process.* **2002**, *74* (3), 355−361.
(7) Mang, D.; Boehm, H. P.; Stanczyk, K.; Marsh, H. Inhibiting effect of incorporated nitrogen on the oxidation of microcrystalline carbons. *Carbon* **1992**, *30* (3), 391−8.
(8) Joseph, S.; Graber, E. R.; Chia, C.; Munroe, P.; Donne, S.; Thomas, T.; Nielsen, S.; Marjo, C.; Rutlidge, H.; Pan, G. X.; Li, L.; Taylor, P.; Rawal, A.; Hook, J. Shifting paradigms: Development of high-efficiency biochar fertilizers based on nano-structures and soluble components. *Carbon Manage.* **2013**, *4* (3), 323−343.
(9) Li, K.; Ling, L.; Lu, C.; Qiao, W.; Liu, Z.; Liu, L.; Mochida, I. Catalytic removal of SO_2 over ammonia-activated carbon fibers. *Carbon* **2001**, *39* (12), 1803−1808.
(10) Bimer, J.; Salbut, P. D.; Berlozecki, S.; Boudou, J.-P.; Broniek, E.; Siemieniewska, T. Modified active carbons from precursors enriched with nitrogen functions: Sulfur removal capabilities. *Fuel* **1998**, *77* (6), 519−525.
(11) Przepiorski, J. Enhanced adsorption of phenol from water by ammonia-treated activated carbon. *J. Hazard. Mater.* **2006**, *135* (1−3), 453−456.
(12) Nakahashi, T.; Konno, H.; Inagaki, M. Chemical state of nitrogen atoms in carbon films prepared from nitrogen-containing polymer films. *Solid State Ionics* **1998**, *113−115*, 73−77.
(13) Iwazaki, T.; Obinata, R.; Sugimoto, W.; Takasu, Y. High oxygen-reduction activity of silk-derived activated carbon. *Electrochem. Commun.* **2009**, *11* (2), 376−378.
(14) Maldonado, S.; Stevenson, K. J. Influence of nitrogen doping on oxygen reduction electrocatalysis at carbon nanofiber electrodes. *J. Phys. Chem. B* **2005**, *109* (10), 4707−4716.
(15) Xia, Y.; Yang, Z.; Mokaya, R. Mesostructured hollow spheres of graphitic N-doped carbon nanocast from spherical mesoporous silica. *J. Phys. Chem. B* **2004**, *108* (50), 19293−19298.
(16) Glerup, M.; Steinmetz, J.; Samaille, D.; Stephan, O.; Enouz, S.; Loiseau, A.; Roth, S.; Bernier, P. Synthesis of N-doped SWNT using the arc-discharge procedure. *Chem. Phys. Lett.* **2004**, *387* (1−3), 193−197.
(17) Titirici, M.-M.; Antonietti, M. Chemistry and materials options of sustainable carbon materials made by hydrothermal carbonization. *Chem. Soc. Rev.* **2010**, *39* (1), 103−116.
(18) Falco, C.; Baccile, N.; Titirici, M.-M. Morphological and structural differences between glucose, cellulose and lignocellulosic biomass derived hydrothermal carbons. *Green Chem.* **2011**, *13* (11), 3273−3281.
(19) Wang, L.; Guo, Y.; Zou, B.; Rong, C.; Ma, X.; Qu, Y.; Li, Y.; Wang, Z. High surface area porous carbons prepared from hydrochars by phosphoric acid activation. *Bioresour. Technol.* **2011**, *102* (2), 1947−1950.
(20) Kabyemela, B. M.; Adschiri, T.; Malaluan, R. M.; Arai, K. Glucose and fructose decomposition in subcritical and supercritical water: detailed reaction pathway, mechanisms, and kinetics. *Ind. Eng. Chem. Res.* **1999**, *38* (8), 2888−2895.
(21) Sevilla, M.; Fuertes, A. B. Chemical and structural properties of carbonaceous products obtained by hydrothermal carbonization of saccharides. *Chem.−Eur. J.* **2009**, *15* (16), 4195−4203.
(22) Zou, S.; Wu, Y.; Yang, M.; Kaleem, I.; Chun, L.; Tong, J. Production and characterization of bio-oil from hydrothermal liquefaction of microalgae *Dunaliella tertiolecta* cake. *Energy (Oxford, U.K.)* **2010**, *35* (12), 5406−5411.
(23) Lynam, J. G.; Toufiq, R. M.; Vasquez, V. R.; Coronella, C. J. Effect of salt addition on hydrothermal carbonization of lignocellulosic biomass. *Fuel* **2012**, *99*, 271−273.
(24) Ming, J.; Wu, Y.; Liang, G.; Park, J.-B.; Zhao, F.; Sun, Y.-K. Sodium salt effect on hydrothermal carbonization of biomass: A catalyst for carbon-based nanostructured materials for lithium-ion battery applications. *Green Chem.* **2013**, *15* (10), 2722−2726.
(25) Zhang, D.; Hao, Y.; Ma, Y.; Feng, H. Hydrothermal synthesis of highly nitrogen-doped carbon powder. *Appl. Surf. Sci.* **2012**, *258* (7), 2510−2514.
(26) Jagadeesan, D.; Eswaramoorthy, M. Functionalized carbon nanomaterials derived from carbohydrates. *Chem.−Asian J.* **2010**, *5* (2), 232−243.
(27) Yao, C.; Shin, Y.; Wang, L.-Q.; Windisch, C. F., Jr.; Samuels, W. D.; Arey, B. W.; Wang, C.; Risen, W. M., Jr.; Exarhos, G. J. Hydrothermal dehydration of aqueous fructose solutions in a closed system. *J. Phys. Chem. C* **2007**, *111* (42), 15141−15145.
(28) Antal, M. J., Jr.; Mok, W. S. L.; Richards, G. N. Kinetic studies of the reactions of ketoses and aldoses in water at high temperature. 2. Four-carbon model compounds for the reactions of sugars in water at high temperature. *Carbohydr. Res.* **1990**, *199* (1), 111−15.
(29) Daorattanachai, P.; Khemthong, P.; Viriya-empikul, N.; Laosiripojana, N.; Faungnawakij, K. Conversion of fructose, glucose, and cellulose to 5-hydroxymethylfurfural by alkaline earth phosphate catalysts in hot compressed water. *Carbohydr. Res.* **2012**, *363*, 58−61.
(30) Li, M.; Li, W.; Liu, S. Hydrothermal synthesis, characterization, and KOH activation of carbon spheres from glucose. *Carbohydr. Res.* **2011**, *346* (8), 999−1004.
(31) Titirici, M.-M.; Antonietti, M.; Baccile, N. Hydrothermal carbon from biomass: a comparison of the local structure from poly- to monosaccharides and pentoses/hexoses. *Green Chem.* **2008**, *10* (11), 1204−1212.
(32) Yu, L.; Falco, C.; Weber, J.; White, R. J.; Howe, J. Y.; Titirici, M.-M. Carbohydrate-derived hydrothermal carbons: A thorough characterization study. *Langmuir* **2012**, *28* (33), 12373−12383.
(33) Falco, C.; Perez, C. F.; Babonneau, F.; Gervais, C.; Laurent, G.; Titirici, M.-M.; Baccile, N. Hydrothermal carbon from biomass: Structural differences between hydrothermal and pyrolyzed carbons via 13C solid state NMR. *Langmuir* **2011**, *27* (23), 14460−14471.
(34) Richards, G. N.; Shafizadeh, F. Mechanism of thermal degradation of sucrose. A preliminary study. *Aust. J. Chem.* **1978**, *31* (8), 1825−32.
(35) Liu, K.; Chen, T. Mechanism of the thermal decomposition of ammonium sulfate. *Huaxue Yanjiu Yu Yingyong* **2002**, *14* (6), 737−738 C3.
(36) Garrote, G.; Dominguez, H.; Parajo, J. C. Hydrothermal processing of lignocellulosic materials. *Holz Roh- Werkst.* **1999**, *57* (3), 191−202.
(37) Tanger, J. C. I. V.; Pitzer, K. S. Calculation of the ionization constant of water to 2,273 K and 500 MPa. *AIChE J.* **1989**, *35* (10), 1631−38.
(38) Daorattanachai, P.; Namuangruk, S.; Viriya-empikul, N.; Laosiripojana, N.; Faungnawakij, K. 5-Hydroxymethylfurfural production from sugars and cellulose in acid- and base-catalyzed conditions under hot compressed water. *J. Ind. Eng. Chem. (Amsterdam, Neth.)* **2012**, *18* (6), 1893−1901.
(39) Baccile, N.; Laurent, G.; Babonneau, F.; Fayon, F.; Titirici, M.-M.; Antonietti, M. Structural characterization of hydrothermal carbon spheres by advanced solid-state MAS 13C NMR investigations. *J. Phys. Chem. C* **2009**, *113* (22), 9644−9654.
(40) Ryu, J.; Suh, Y.-W.; Suh, D. J.; Ahn, D. J. Hydrothermal preparation of carbon microspheres from mono-saccharides and phenolic compounds. *Carbon* **2010**, *48* (7), 1990−1998.
(41) March, J. *Advanced Organic Chemistry, Reactions, Mechanisms, and Structure*, 4th ed.; John Wiley and Sons: New York, 1992.
(42) Sidgwick, N. V. The Organic Chemistry of Nitrogen. Oxford University Press: Oxford, U.K.1966; pp 619−703.